Letter to the Editor

Posttransplant molecular Burkitt lymphomas are frequently *MYC*-negative and characterized by the 11q-gain/loss pattern

Julio Finalet Ferreiro,[1] Julie Morscio,[2] Daan Dierickx,[3] Lukas Marcelis,[2] Gregor Verhoef,[3] Peter Vandenberghe,[1] Thomas Tousseyn,[2] and I Wlodarska[1]

[1]KU Leuven, University of Leuven, Center for Human Genetics, Leuven, Belgium;

[2]KU Leuven, University of Leuven, Translational Cell and Tissue Research and KU Leuven, University Hospitals Leuven, Department of Pathology, Leuven, Belgium;

[3]KU Leuven, University Hospitals Leuven, Department of Hematology, Leuven, Belgium

Running head: Posttransplant Burkitt lymphoma

Correspondence: Iwona Wlodarska, iwona.wlodarska@uzleuven.be

Word count:

Text: 1488

Tables: 2

Figure: 1

Supplemental file: 1

Acknowledgements

The authors would like to thank Ursula Pluys, Kathleen Doms and Emilie Bittoun for their excellent technical assistances and Rita Logist for the editorial help. This study was supported by the concerted action grant from the K.U.Leuven no. 3M040406 (T.T, P.V, and I.W) (http://www.kuleuven.be/), research grants from “Stichting tegen Kanker” (PV) (http://www.kanker.be/) and the FWO-Vlaanderen (G081411N to G.V. and T.T). P.V. is a senior clinical investigator of the FWO-Vlaanderen (http://www.fwo.be/en/). T.T

holds a Mandate for Fundamental and Translational Research from the “Stichting tegen Kanker” (2014-083).

The study was approved by the Ethical Committee of the University Hospitals Leuven.

Burkitt lymphoma (BL) is a biologically and molecularly defined tumor hallmarked by *IG*-mediated t(8q24) resulting in upregulation of *MYC*.[1,2] Recent studies of 59 molecular BL (mBL) identified a novel aberration manifested by a specific 11q-gain/loss pattern in two cases (3%) lacking *MYC* translocation.[3] The aberration was subsequently detected in 15 MYC-negative high-grade B-cell lymphomas resembling BL and two cell lines derived from high-grade B-cell lymphomas. Further studies defined the minimal gained and lost regions at 11q23.3 and 11q24.1qter, respectively, and identified candidate genes potentially affected by these imbalances: the constantly overexpressed *PAFAH1B2*/11q23.3, and *FLI1* (downregulated) and *ETS1* (recurrently mutated) targeted by a homozygous 11q24 microdeletion.

We provide here evidence that this peculiar 11q-gain/loss aberration is particularly frequent in BL in immunodeficient hosts, as it was identified in three out of seven patients with mBL after solid organ transplantation and under immunosuppressive maintenance. The cases were selected from a cohort of 174 posttransplant patients diagnosed with posttransplant lymphoproliferative disorders (PTLD) between 1989 and 2012 at the University Hospitals of KU Leuven (Leuven, Belgium). This cohort mainly comprised diffuse large B-cell lymphoma (75%).[4,5] Other entities were less frequent and included plasmacytoma and plasmablastic non-Hodgkin lymphoma (NHL),[6] T-cell NHL,[7] BL, small cell B-NHL and unspecified cases. The seven posttransplant BL (PT-BL) cases reported here were analysed using conventional cytogenetics, array CGH (aCGH), FISH, immunohistochemistry (IHC), gene expression profiling (GEP) and bioinformatics (Supplementary information). As controls, we included four cases of typical *MYC*-translocation-positive BL from immunocompetent hosts (IC-BL). All cases fulfilled the morphological and immunological criteria of BL defined by the 2008 WHO classification[8] (Table 1).

Relevant clinical, pathologic and cytogenetic features of the studied cases are summarized in Table 2. The PT-BL patients, all men, had undergone liver (n=3), heart (n=2) or kidney (n=2) transplantation. The median age at time of PTLD was 47.5 years (range, 15-70 years). Five cases were EBV-negative and two adolescent cases (no. 3 and 4) were EBV-positive. Patients developed BL after a median interval of 40.7 months (range, 11-66 months) following transplantation. The interval was significantly shorter for EBV-positive cases than EBV-negative cases (12 *vs* 52.2 months, respectively). All seven patients were treated with either rituximab and/or CHOP. Most of them achieved complete remission but four patients died within 4-11 months after diagnosis (average 6 months), including two patients (no. 6 and 7) who died due

to disease-related complications. Three patients are alive, including both EBV-positive patients, and their survival ranges from 34 to 99 months (median 70 months) (Table 2). Based on a global gene expression pattern, all seven PT-BL cases (as well as control IC-BL cases) showed molecular profile of BL and were readily distinguished from PT-/IC-DLBCL[5] using two mBL classifiers[1,2] (Supplementary Figure 1). Cytogenetics and/or FISH demonstrated t(8q24/*MYC*) in four PT-mBLs, while three cases (no. 5-7, all EBV-negative) appeared to be *MYC*-translocation-negative. Interestingly, karyotypes of the two latter cases revealed various 11q aberrations, which after additional FISH analysis (data not shown) were described as der(11)(11pter->11q23.3::11q23.3->11q13::8q22q24.3) and der(11)t(11;18)(q23.3;q12) (Figure 1A). Array CGH analysis performed in all 11 cases detected the characteristic 11q-gain/loss pattern in the three *MYC*-translocation-negative cases (Figure 1B). This pattern was associated with a dup(11)(q13q23.3) in case 5, focal gain-and-amplification of ~4Mb region at 11q23.3 in case 6 (confirmed by FISH, Figure 1C, Supplementary Figure 2) and complex 11q imbalances in case 7 (Table 2). Interestingly, dup(11)(q13q23.3) identified in case 5 was associated with an inversion, like in several previously reported cases.[3,9] Losses, resulting from different nonreciprocal translocations in cases 5 and 6, constantly targeted the 11q23.3/q24.1qter region. Homozygous deletions were not detected. The aCGH data allowed to define the minimal gained region (MGR) (~4Mb) and minimal lost region (MLR) (~13.5Mb) which were mapped at 11q23.3 (chr11:116072765-120087526bp (hg19)) and 11q24.1q25 (chr11:121499571-135006516bp (hg19)), respectively. Notably, *MYC*-translocation-positive PT-mBL cases had either a balanced karyotype, or were featured by 2-9 additional imbalances, including subclonal gains/losses, similar like IC-mBL cases (Table 2). The latter ones, however, showed a frequent gain of chromosome 7 (60%), not seen in PT-mBL cases.

In order to identify genes affected by the 11q imbalances, we compared GEPs of cases 5-7 (11q-gain/loss-positive) and cases 1-4 (*MYC*-translocation-positive), and focused on genes harboured by MGR (69 genes) and MLR (106 genes). Altogether, 33 genes with a differential expression were identified: 15 at MGR (all upregulated) and 18 at MLR (all downregulated) (Supplementary Table 1). The most significantly upregulated was *USP2* (ubiquitin specific peptidase 2) showing up to 30.6-fold higher expression in *MYC*-translocation-negative cases than in *MYC*-translocation-positive cases (Supplementary Figure 3). Differential expression of the remaining MGR genes was much lower (1.35-2.75-fold). Level of

differentially downregulated genes ranged from -1.32 to -2.35-fold. Notably, both regions harbor several genes which might be implicated in the pathogenesis of *MYC*-translocation-negative mBL. Particularly interesting are two oncogenes, *USP2* and *CBL*, and the previously discussed *PAFAH1B2* located in MGR.[3] USP2, which was the most significantly upregulated in 11q-gain/loss-positive mBLs, acts as a modulator of TNFα-induced NF-kB signaling and prolongs the half-life of targets such as fatty acid synthase, MDM2 and MDM4/MDMX (negative regulators of p53) and cyclin D1 (G1/S transition). The enzyme, like other deubiquitinases, in implicated in cancer, particularly in prostate carcinomas (reviewed by Fraile *et al*.[10]). In MLR, dysregulated genes comprise two candidate tumor suppressor genes, *TBRG1* and *EI24*, and five genes either related to cancer or involved in cancer-related processes, including *ETS1*, *TIRAP*, *ST14*, *NCAPD3* and *ZNF202*. Noteworthy, *FLI1*, the candidate target gene,[3] was not differentially downregulated in our cases (Supplementary Figure 3). Hierarchical clustering of the studied cases using the set of 11q23/q24 dysregulated genes showed that *MYC*-translocation-negative PT-mBL cases cluster together and separate from *MYC*-translocation-positive PT-/IC-mBL (Figure 1D).

PT-mBL cases with the 11q-gain/loss pattern revealed a lower expression of *MYC* mRNA than *MYC*-translocation-positive cases (Supplementary Figure 3). Using IHC with MYC antibody (clone Y69; Epitomics, Burlingame, CA), all studied mBL cases showed highly variable expression of MYC protein, which has not necessarily correlated with rearrangement of *MYC* (Table 1) (Supplementary Figure 4). These results, however, remain in line with the recently published data of Chisholm et al.[11]

To examine whether the 11q-gain/loss aberration also features BL and/or DLBCL cases from immunocompetent patients collected in our institution, we analyzed by FISH two known cases of *MYC*-translocation-negative BL and five cases of *MYC*-translocation-negative DLBCL harbouring 11q aberrations (mostly dup(11q)). Using the designed 11q23/q24 assay covering MGR and MLR (Supplementary Figure 2), the 11q-gain/loss pattern was detected in one of two *MYC*-translocation-negative BL case (data not shown). The second BL case showed a normal FISH pattern, while all five DLBCLs revealed gain of 11q23.3, without, however, an associated loss of 11q24. These findings confirm a rare occurrence of the 11q-gain/loss pattern in IC-BL/-DLBCL.

To unravel biological consequences of the 11q-gain/loss aberration in mBL, we explored the MGR/MLR-dysregulated genes using Ingenuity Pathway Analysis (IPA) (see Supplementary Methods).

IPA showed that the genes are implicated in important biological processes, including cancer, and the majority of them (22/33) are involved in the TP53 and MYC networks, frequently by direct protein-protein interactions (Figure 1E). These findings and the observation that cases with 11q imbalances cluster with *MYC*-translocation-positive mBL (using two mBL classifiers[1,2]) suggest that the 11q-gain/loss aberration is a 'molecular variant' of t(8q24/*MYC*) affecting the same or overlapping pathological pathways. Similar phenomenon has been recently described in BCR-ABL-negative Ph-like ALL showing a spectrum of kinase-activating alterations.[12] The astonishing consistency of the 11q-gain/loss pattern suggests that the driving potential of this aberration results from a concerted overexpression of the defined 11q23.3 genes, including *USP2, CBL* and *PAFAH1B2,* and simultaneous downregulation of 11q24q25 genes, among others *TBRG1, EI24* and *ETS1*. Interestingly, a similar gain-and-loss pattern has been identified in hepatosplenic T-cell lymphoma characterized by a constant 7p14.1p22.1-loss/7q22.11q31.1-gain pattern[13], which, noteworthy, is frequently observed in immunosuppressed patients.

PTLD is typically an EBV driven process and our recent study of 33 PT-DLBCL (72% EBV-positive and 28% EBV-negative) led to conclusion that EBV-negative PT-DLBCL were coincidental lymphomas in immunosuppressed patients.[5] Among the reported PT-mBLs, only 30% of cases were EBV-positive and they clustered together with EBV-negative PT-mBL and IC-mBL (Supplementary Figure 1). These findings are in line with observations of Piccaluga *et al.*,[14] who found that all three BL subtypes, sporadic, endemic and HIV-positive, share a common gene expression signature, distinct from other B-cell malignancies, and suggested that not EBV, but MYC-dependent signature had a major effect on the clustering.

Altogether, we confirmed a recurrent occurrence of the 11q-gain/loss pattern in high grade B-cell lymphoma and showed that this aberration is significantly more frequent (p-value <0.007, Fisher's exact test) in BL occurring in the setting of transplantation and immunosuppression (43% of all PT-mBL and 60% of EBV-negative PT-mBL) than in immunocompetent patients (3%)[1], suggesting that immunosuppression may favour its formation. Further studies of PT-BL are needed to confirm this association. As identification of patients with the 11q-gain/loss aberration is clinically important but cytogenetically challenging, we recommend the designed 11q-MGR/MLR FISH assay as a useful diagnostic tool to evaluate both, posttransplant- and immunocompetent BL patients.

Conflict-of-interest

The authors declare no conflict of interest.

Author contributions

J.F.F., J.M., T.T. and I.W. designed the research. J.F.F., J.M., L.M., T.T., and I.W. performed the research and analyzed the data. D.D., G.V. and P.V. provided samples and clinical data. J.F.F., J.M., T.T. and I.W. generated figures and wrote the paper.

Supplementary information is available at the Haematologica website.

References

1. Dave SS, Fu K, Wright GW, et al. Molecular diagnosis of Burkitt's lymphoma. N Engl J Med. 2006;354(23) :2431-2442.
2. Hummel M, Bentink S, Berger H, et al. A biologic definition of Burkitt's lymphoma from transcriptional and genomic profiling. N Engl J Med. 2006;354(23) :2419-2430.
3. Salaverria I, Martin-Guerrero I, Wagener R, et al. A recurrent 11q aberration pattern characterizes a subset of MYC-negative high-grade B-cell lymphomas resembling Burkitt lymphoma. Blood. 2014;123(8) :1187-1198.
4. Dierickx D, Tousseyn T, Sagaert X, et al. Single-center analysis of biopsy-confirmed posttransplant lymphoproliferative disorder: incidence, clinicopathological characteristics and prognostic factors. Leuk Lymphoma. 2013;54(11) :2433-2440.

5. Morscio J, Dierickx D, Ferreiro JF, et al. Gene expression profiling reveals clear differences between EBV-positive and EBV-negative posttransplant lymphoproliferative disorders. Am J Transplant. 2013;13(5) :1305-1316.

6. Morscio J, Dierickx D, Nijs J, et al. Clinicopathologic comparison of plasmablastic lymphoma in HIV-positive, immunocompetent, and posttransplant patients: single-center series of 25 cases and meta-analysis of 277 reported cases. Am J Surg Pathol. 2014;38(7) :875-886.

7. Herreman A, Dierickx D, Morscio J, et al. Clinicopathological characteristics of posttransplant lymphoproliferative disorders of T-cell origin: single-center series of nine cases and meta-analysis of 147 reported cases. Leuk Lymphoma. 2013;54(10) :2190-2199.

8. Swerdlow SH, Campo E, Harris NL, et al. WHO Classification of tumours of Haematopoietic and Lymphoid Tissues. Lyon: International Agency for Research on Cancer, 2008.

9. Pienkowska-Grela B, Rymkiewicz G, Grygalewicz B, et al. Partial trisomy 11, dup(11) (q23q13) , as a defect characterizing lymphomas with Burkitt pathomorphology without MYC gene rearrangement. Med Oncol. 2011;28(4) :1589-1595.

10. Fraile JM, Quesada V, Rodriguez D, Freije JM, Lopez-Otin C. Deubiquitinases in cancer: new functions and therapeutic options. Oncogene. 2012;31(19) :2373-2388.

11. Chisholm KM, Bangs CD, Bacchi CE, Kirsch HM, Cherry A, Natkunam Y. Expression Profiles of MYC Protein and MYC Gene Rearrangement in Lymphomas. Am J Surg Pathol. 2015;39(3) :294-303.

12. Roberts KG, Li Y, Payne-Turner D, et al. Targetable kinase-activating lesions in Ph-like acute lymphoblastic leukemia. N Engl J Med. 2014;371(11) :1005-1015.

13. Finalet FJ, Rouhigharabaei L, Urbankova H, et al. Integrative genomic and transcriptomic analysis identified candidate genes implicated in the pathogenesis of hepatosplenic T-cell lymphoma. PLoS One. 2014;9(7) :e102977.

14. Piccaluga PP, De FG, Kustagi M, et al. Gene expression analysis uncovers similarity and differences among Burkitt lymphoma subtypes. Blood. 2011;117(13) :3596-3608.

Table 1. Morphology and immunophenotype of the reported postransplant and immunocompromised BL cases.

Case	Localization	Morphology	Immunohistochemistry									EBV latency profile
			CD20	CD10	MYC (%)	TdT	BCL2	BCL6	MUM1	Ki67 (%)	EBER	
MYC-translocation-positive PT-mBL												
1	LN	medium and large-sized cells, limited starry sky	pos	pos	0		pos[a]	pos	neg	100	neg	
2	LN	large-sized cells, starry sky	pos	pos	35	neg	neg	pos	neg	100	neg	
3	GALT	medium-sized cells, starry sky	pos	pos	100		neg	pos	neg	95	pos	intermediate
4	LN	medium-sized cells, starry sky	pos	pos	100	neg	neg	pos	neg	95	pos	intermediate
MYC-translocation-negative PT-mBL												
5	WR	large-sized cells, starry sky	pos	pos	0	neg	neg	pos	neg	90	neg	
6	LN	medium-sized cells, starry sky	pos	pos	25 (w)	neg	neg	pos	neg	99	neg	
7	T	large-sized cells, starry sky	pos	pos	75 (w)		neg	pos	neg	99	neg	
MYC-translocation-positive IC-mBL												
8	GALT	large-sized cells, starry sky	pos	pos	50	neg	neg	pos	pos	100	neg	
9	LN	medium-sized cells, starry sky	pos	pos	90	neg	neg	pos	pos	100	neg	
10	LN	medium-sized cells, limited starry sky	pos	pos	0	neg	neg	pos	neg	90	neg	
11	LN	medium-sized cells, starry sky	pos	pos	25	neg	neg	pos	neg	95	neg	

[a] normal FISH *BCL2* pattern

PT, posttransplant; IC, immunocompetent; mBL, molecular Burkitt lymphoma; LN, lymph node; GALT, gut associated lymphoid tissue; WR, Waldeyer ring; T, testis; pos, positive; neg, negative; w, weak

Table 2. Relevant clinical, pathologic and genetic data of the reported posttransplant and immunocompetent BL cases.

Case	Age/ Sex	Immune status	Graft	Immuno-suppression	TX-PTDL interval (months)	Stage	EBV	Treatment	Response	Outcome (months)	Cytogenetic and FISH findings	aCGH imbalances (>4Mb) [a]	
												Gains	Losses
MYC-translocation-positive PT-mBL													
1	65/M	ID	heart	CNI+AM	61	IIIA	-	R	CR	D/du (11)	47-48,XY,dup(1)(q21q32)[8],t(8;14)(q24;q32),+12[3],del(13)(q14q22)[cp20]. nuc ish(MYCx2)(5'MYC sep 3'MYCx1)[150/200]	1p11.2q32.1	13q14.13q31.1
2	70/M	ID	liver	CNI	31	IVA	-	CHOP/ R	CR	D/dr (4)	46,XY,del(6)(q23),t(8;22)(q24;q11), inc[15].nuc ish(MYCx2)(5'MYC sep 3'MYCx1)[33/200]	NF	NF
3	16/M	ID	kidney	CNI+AM+CS	13	IVA	+	CHOP/ R	CR	A (34)	NM.nuc ish(MYCx2)(5'MYC sep 3'MYCx1)[160/200]	1q21.2q25.3; 3q27.2q29; 12p13.33p11.22; 12q14.1q24.21; 13q31.1q31.3; 15q24.3q26.2	16p13.3p13.3
4	15/M	ID	liver	CNI+AM+CS	11	IIIA	+	Intensive CT	CR	A (79)	NM.nuc ish(MYCx2)(5'MYC sep 3'MYCx1)[190/200]	no	no
MYC-translocation-negative PT-mBL													
5	54/M	ID	heart	CNI+AM	66	IIA	-	CHOP/ R	CR	A (99)	44-47,XY,add(7)(p22)[3],der(11)(11pter->11q23.3::11q23.3->11q13::8q22q24.3),+1-2mar[cp5].nuc ish(MYCx2)[200]	8q22.3q24.23; 11q13.1q23.3; 12p13.32q13.13	8p23.3p23.2; 8q12.1q13.1; 11q23.3q25; 20q11.23q13.13; 21q21.1q21.2
6	68/M	ID	liver	CNI	46	IA	-	CHOP/ R	PD	D/dr (4)	42-44,XY,-4,add(10)(p11), der(11)t(11;18)(q23.3;q12)[cp4].nuc ish(MYCx2)[200]	11q23.3q23.3; 16q21.1q24.3; 18q12.1q23	4p16.3q35.2; 10p15.3p11.4; 11q23.3q25; 20q11.23q13.33
7	44/M	ID	kidney	CNI+AM	57	IVB	-	CHOP/ R	CR	D/dr (5)	ND.nuc ish(MYCx2)[200]	2q23.3q37.3; 7q32.3q36.3; 11p15.4p15.1; 11q13.4q14.1; 11q22.3q24.1; 12p13.33q24.33; 13q32.1q34; 17q22q23.2	11q14.1q22.3; 11q24.1q25; 13q31.1q32.1;

MYC-translocation-positive IC-mBL													
8	77/M	IC	-	-	-	IA	-	CHOP	CR	D/du (105)	ND.nuc ish(MYCx2)(5'MYC sep 3'MYCx1) [55/100]	3p26.3q12.2; 3q26.33q27; 18q12.1q23	3q13.11q26.32; 20q11.23q13.12
9	36/M	IC	-	-	-	IIIB	-	Intensive CT	CR	A (98)	ND.nuc ish(MYCx2)(5'MYC sep 3'MYCx1) [80/100]	no	no
10	18/M	IC	-	-	-	IVB	-	CHOP/ R	CR	A (106)	ND. nuc ish(MYCx2)(5'MYC sep 3'MYCx1)[62/100]	7p22.3q36.3; 12p13.33q24.33; 21q11.2q22.3	1p36.33p36.23; 2q21.2q24.1; 4q21.1q21.23
11	75/M	IC	-	-	-	IVB	-	CHOP/ R	CR	A (45)	ND.nuc ish(MYCx2)(5'MYC sep 3'MYCx1) [65/100]	7p22.3q36.3; 8q22.3q24.3; 9q21.11q34.3	5q35.2q35.3; 6q12q16.3

[a,] mosaic/subclonal regions are underlined

PT, posttransplant; IC, immunocompetent; mBL, molecular Burkitt lymphoma; M, male; ID, immunodeficient; IC, immunocompetent; CNI, calcineurin inhibitor; AM, antimetabolite; CS, low dose corticosteroids; TX, transplantation; PTLD, posttransplant lymphoproliferative disorder; EBV, Epstein-Barr virus; CHOP, cyclophosphamide, doxorubicin, vincristine and prednisone; CT, chemotherapy; R, rituximab; CR, complete remission; PD, progressive disease; A, alive; D/du, dead, disease unrelated; D/dr, dead, disease related; NM, no mitosis; ND, not done; NF, not informative

Legend to the Figure

Figure 1. Genomic and transcriptomic data on PT-mBL. (**A**) Partial karyotype of case 5 (c5) and case 6 (c6) showing chromosome 11 abnormalities and FISH images of both derivative chromosomes painted with WCP11 (green) and WCP8 (red) (case 5), and WCP18 (red) (case 6). The aberrations were eventually described as der(11)(11pter->11q23.3::11q23.3->11q13::8q22q24.3) and der(11)t(11;18)(q23.3;q12), respectively. Note (inverted) duplication of 11q13q23.3 in case 5 and a normal appearance of this region in case 6. (**B**) Chromosomal view of chromosome 11q23q24 and imbalances identified by aCGH analysis in cases 5-7. Gained regions are highlighted in red-scale (increased intensity reflects an increased amplification level), while lost regions are marked in green. Note a variable level of 11q23.3 gain, a common loss of 11q24qter and the defined MLR (~4 Mb) and MLR (~13.5 MB). (**C**) Examples of interphase FISH analysis performed in case 5 (a) and case 6 (b, c). The applied probes include the 11q-MGR/MLR FISH assay (a) (b), and two probes from the duplicated (RP11-284O21-SpectrumOrange) and amplified (RP11-784K23-SpectrumGreen; Supplementary Figure 2) area in case 6 (c). Note the duplicated and amplified red/11q23.3 signal in (a) and (c), respectively, and loss of the green/11q24 signal in both cases. In (c), note two red and five green signals in the cluster, illustrating various levels of gain within MGR. (**D**) Hierarchical clustering of mBL cases using the dysregulated genes located in the MGR and MLR. (**E**) Interaction network found by IPA involving genes targeted by the 11q-gain/loss aberration (bold edges). Solid and interrupted lines represent direct and indirect interactions, respectively. Notably, most of the interactions in this network are direct protein-protein interactions. The molecules with blue and green edges are encoded by MGR- and MLR-associated genes, respectively. The data obtained by comparison of cases 5-7 (PT-mBL with the 11q-gain/loss pattern) (11q+/-) and cases 1-4 (PT-*MYC*-translocation-positive mBL) (t(*MYC*) were overlaid in this network. Molecules which are down- and upregulated in cases with 11q+/- when compared to cases with t(*MYC*) are filled in green and red, respectively.

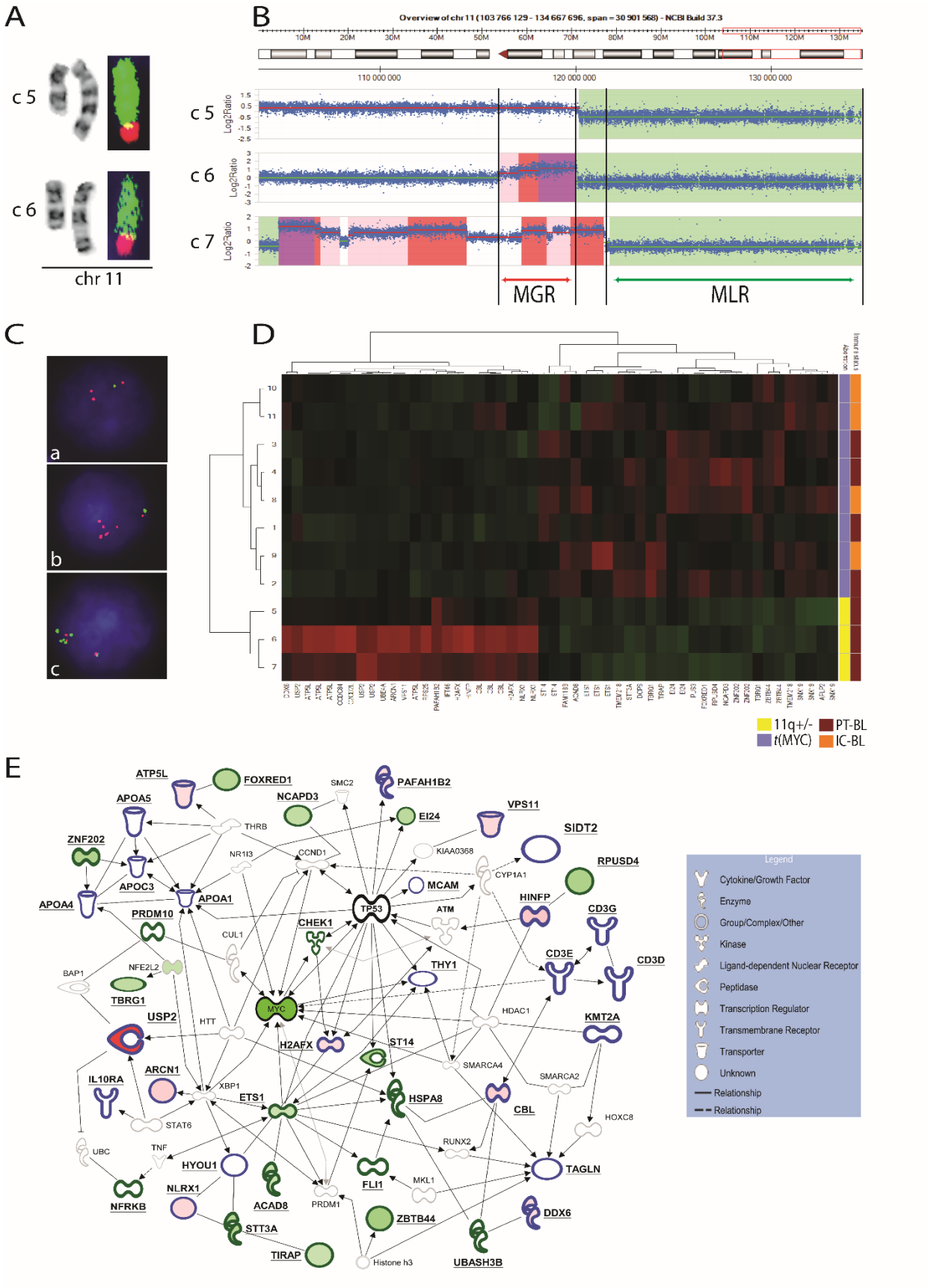
A
c 5
c 6
chr 11
B
Overview of chr 11 (103 766 129 - 134 667 696, span = 30 901 568) - NCBI Build 37.3
c 5
c 6
c 7
Log2Ratio
MGR
MLR
C
a
b
c
D
11q+/-
t(MYC)
PT-BL
IC-BL
E
ATP5L
FOXRED1
APOA5
NCAPD3
PAFAH1B2
VPS11
SIDT2
ZNF202
EI24
RPUSD4
APOC3
APOA1
APOA4
MCAM
HINFP
CD3G
PRDM10
CHEK1
TP53
ATM
CD3E
CD3D
THY1
TBRG1
USP2
MYC
HDAC1
KMT2A
H2AFX
ST14
SMARCA4
SMARCA2
ARCN1
IL10RA
HSPA8
CBL
HOXC8
ETS1
STAT6
RUNX2
HYOU1
TAGLN
NLRX1
FLI1
NFRKB
ACAD8
PRDM1
ZBTB44
DDX6
STT3A
TIRAP
Histone h3
UBASH3B
Legend
Cytokine/Growth Factor
Enzyme
Group/Complex/Other
Kinase
Ligand-dependent Nuclear Receptor
Peptidase
Transcription Regulator
Transmembrane Receptor
Transporter
Unknown
Relationship
Relationship

Supplementary information

Supplementary Methods

Cytogenetics and FISH

G-banding chromosomal analysis and fluorescence *in situ* hybridization (FISH) followed routine methods. DNA probes, Bacterial Artificial Clones (BAC), applied for FISH were selected from www.Oct29012.archive.ensembl.org (Supplementary Figure 2). The probes were labeled with SpectrumOrange- and SpectrumGreen-d-UTP (Abbott Molecular, Ottigne, Belgium) using random priming. FISH images were acquired with a fluorescence microscope equipped with an Axiophot 2 camera (Carl Zeiss Microscopy, Jena, Germany) and a MetaSystems ISIS imaging system (MetaSystems, Altlussheim, Germany). In each experiment up to 8 abnormal metaphases and/or 200 interphase cells were evaluated.

High resolution array Comparative Genome Hybridization (aCGH)

Total genomic DNA was isolated from fresh frozen lymphoma samples using standard procedures. Genomic profiling, following the manufacturer's protocols, was performed using the Affymetrix Cytogenetic array 2.7M (www.affymetrix.com). The initial data analysis was performed with the software "Chromosome Analysis Suit" (CHAS) and subsequent analysis (segmentation and aberration heatmap) were performed using the software "ArrayStudio" (www.omicsoft.com). Array CGH data are available at GEO (http://www.ncbi.nlm.nih.gov/projects/geo/query/acc.cgi?acc=GSE64086).

Gene Expression profiling and pathway analysis

Total RNA extraction was performed using TRIzol LS Reagent (Life Technologies Europe B.V., Gent, Belgium). The HG-U133 Plus 2.0 Affymetrix platform (www.affymetrix.com) was used and the raw data (CEL files) were normalized using the GeneChip-Robust Multiarray Averaging (GC-RMA) algorithm. Hierarchical clustering was applied to detect relationship in the data and to identify outliers. To find differentially expressed genes, the General Linear Model (GLM) module of ArrayStudio was used for inference analysis. (www.omicsoft.com). Gene expression data are available at GEO (http://www.ncbi.nlm.nih.gov/projects/geo/query/acc.cgi?acc=GSE64086).

The cases were classified using two molecular gene signatures of BL described by Hummel *et al.* 2006[1] and Dave *at al.* 2006.[2] As a control group, we selected 29 previously studied cases of DLBCL

which were analyzed with the same Affymetrix platform.[3] To group the cases using hierarchical clustering, we used the Ward and Manhattan methods for the linkage and distance, respectively. The clustering of the probes was done using complete link and Pearson's correlation (see details: http://www.arrayserver.com/wiki/index.php?title=HierarchicalClustering).

To identify 11q genes dysregulated in ID-BL with 11q-gain/loss pattern (11q+/-), we performed inference analysis comparing three cases with 11q+/- *versus* four cases of *MYC*-translocation positive BL (t(MYC)). To find significant enriched pathways and biological functions in ID-BL with 11q+/-, we uploaded the result of the inference analyses into the "Ingenuity Pathway Analysis" application (IPA, www.ingenuity.com). From the three confidence levels provided by the system, we used "Experimentally observed" and "Highly predicted" data. For details see: http://ingenuity.force.com/ipa/articles/Tutorial/Tutorials.

Statistical analysis

Association between categorical variables was tested by the Fisher's exact test. *P*-value <0.005 was considered statistically significant.

Immunohistochemistry and chromogenic in situ hybridization

Immunohistochemical stainings were performed on paraffin-embedded sections. All antisera were ready to use antibodies purchased from DAKO (DAKO, Carpinteria, USA) except for C-MYC (Y69, Epitomics, Abcam, Burlingame, CA, USA) and stained in automated fashion according to the manufacturer's recommendations. IHC results were visualized using the OptiView DAB IHC Detection Kit (Ventana, Oro Valley, Tucson, Arizona). Image acquisition was done through a Leica microscope at 200x and 100x magnification. Images were assembled using Adobe Photoshop CS5.

Chromogenic EBER (EBV-encoded RNA) in situ hybridization is considered the standard for diagnosis of EBV-infection and was performed using a 30-mer digoxigenin-labeled oligonucleotide probe (Research Genetics, Huntsville, AL), according to manufacturer's instructions. A control poly-A probe (Ventana Roche, Arizona USA) was used to check for RNA integrity and a proven EBV-driven lymphoma was used as a positive control.

Supplementary references

1. Hummel M, Bentink S, Berger H, et al. A biologic definition of Burkitt's lymphoma from transcriptional and genomic profiling. N Engl J Med. 2006;354(23):2419-2430.
2. Dave SS, Fu K, Wright GW, et al. Molecular diagnosis of Burkitt's lymphoma. N Engl J Med. 2006;354(23):2431-2442.
3. Morscio J, Dierickx D, Ferreiro JF, et al. Gene expression profiling reveals clear differences between EBV-positive and EBV-negative posttransplant lymphoproliferative disorders. Am J Transplant. 2013;13(5):1305-1316.
4. Salaverria I, Martin-Guerrero I, Wagener R, et al. A recurrent 11q aberration pattern characterizes a subset of MYC-negative high-grade B-cell lymphomas resembling Burkitt lymphoma. Blood. 2014;123(8):1187-1198.

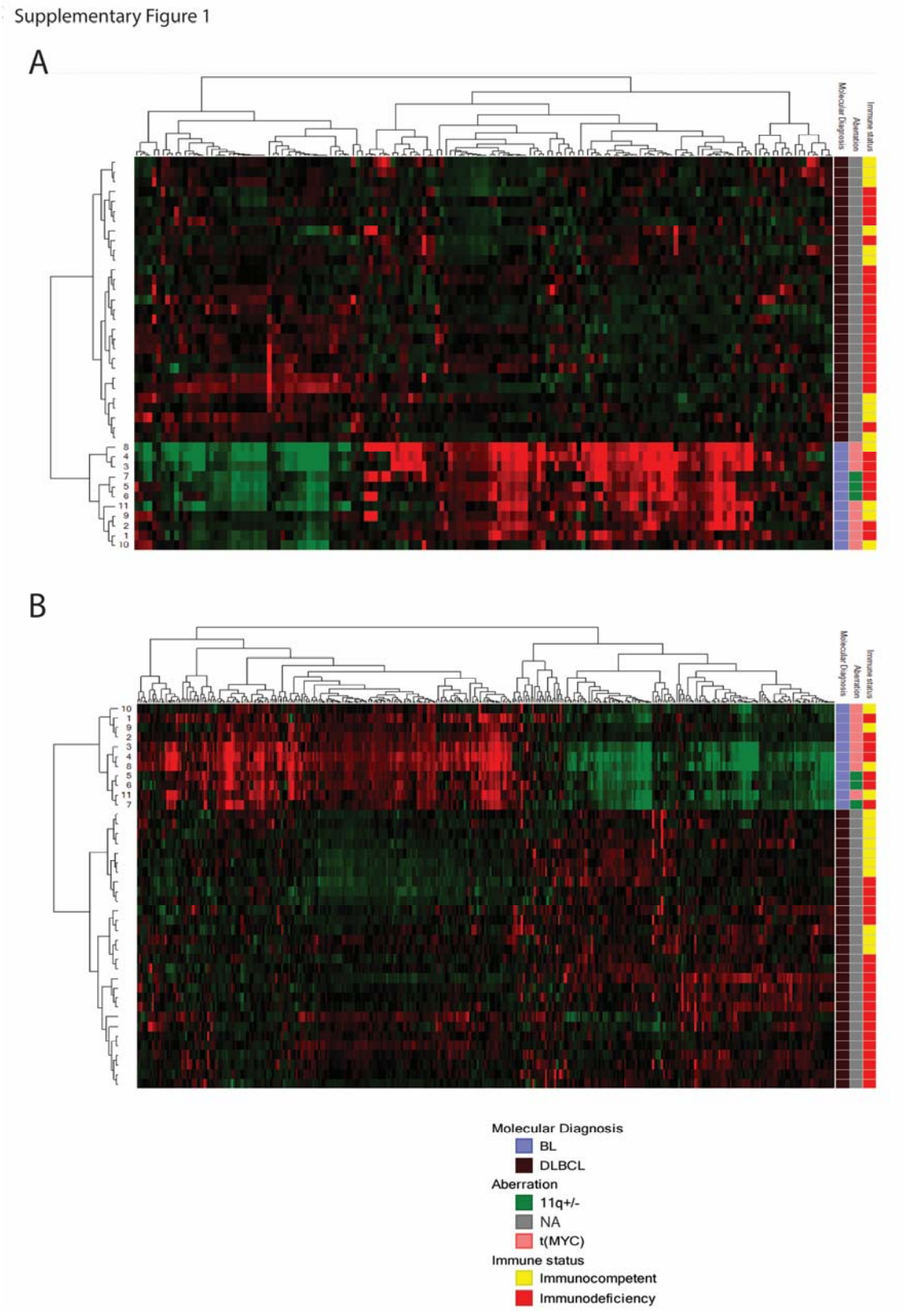

Supplementary Figure S1. Validation of the molecular features of 11 studied BL cases. Hierarchical clustering using the BL signatures from Hummel *et al*. 2006[1] (A) and Dave et al.[2] (B). All cases clustered together and were separated from 19 IC-DLBCL and 10 PT-DLBCL.[3] These data were collected from our microarray experiment in which we used the HG-U133 Plus 2.0 Affymetrix platform. In this platform the gene annotation is based on the genome build Hg19.

Supplementary Figure 2

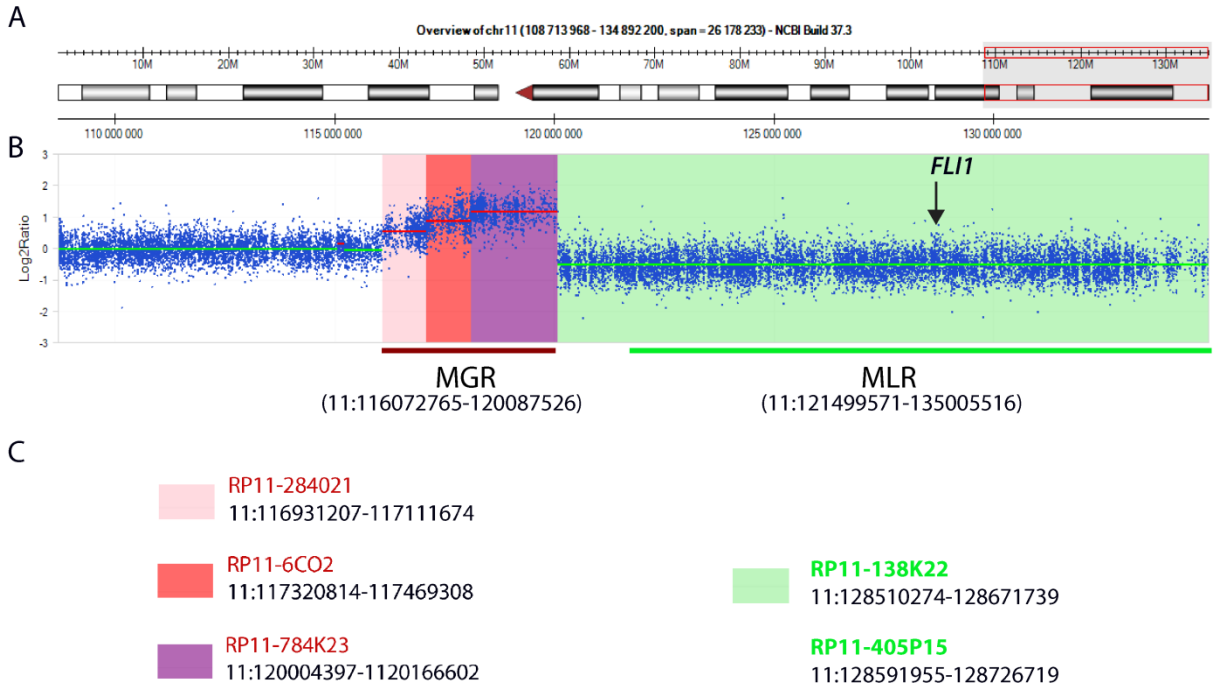

Supplementary Figure S2. Design of the 11q-MGR/MLR FISH assay. (A) View of chromosome 11 with the indicated 11q23.3qter region; (B) 11q imbalances detected by aCGH in case 6, which showed the smallest region of gain (~4 Mb); (C) Selected bacterial artificial chromosome (BAC) clones (www.Oct2012.archive.ensembl.org) and their genomic localization. Note that the assay comprises three MGR-related BAC clones (labeled with SpectrumOrange-d-UTP, shown in red-scale) representing three differentially gained areas in case 6 and two clones spanning *FLI1* (labeled with SpectrumGreen-d-UTP, shown in green), the gene targeted by biallelic deletion on one case reported by Salaverria et al.[4]

Supplementary Figure 3

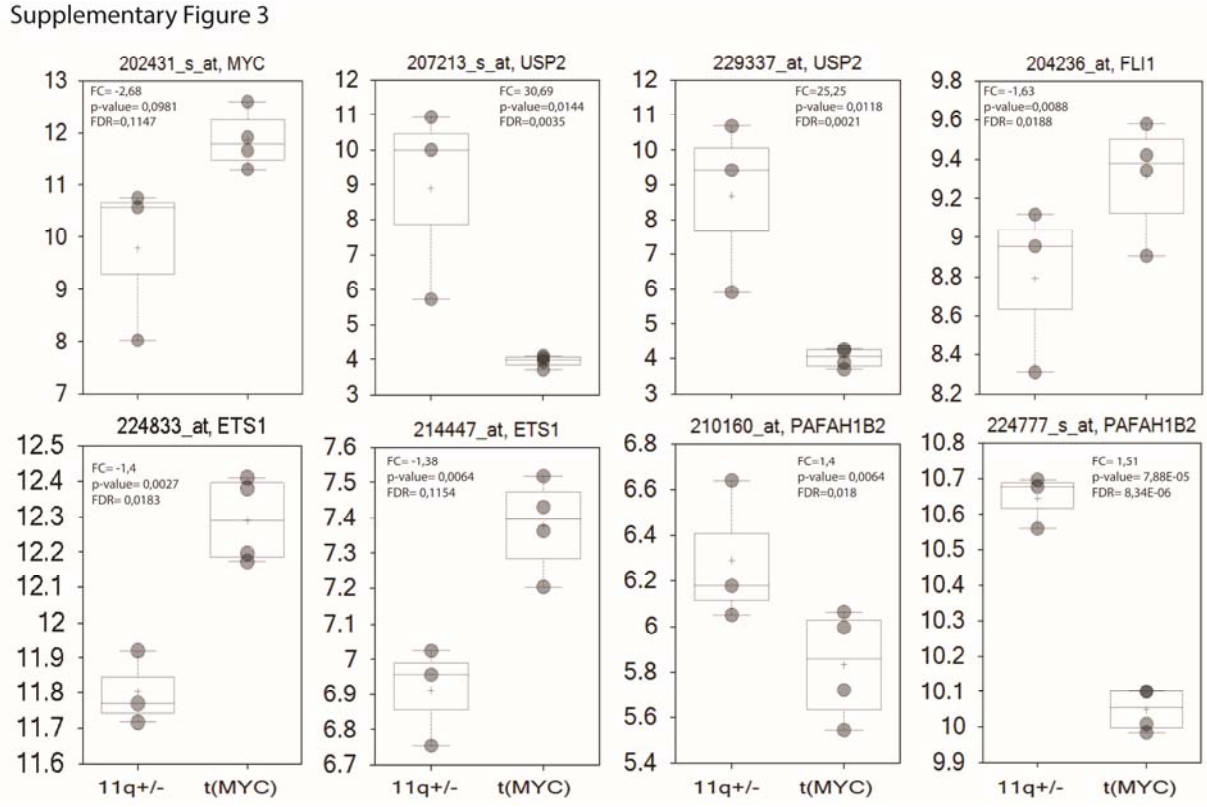

Supplementary Figure S3. Expression value of selected genes. Normalized signal values of array probes covering *USP2, ETS1, PAFAH1B2, FLI1* and *MYC*. The p-value and the "corrected-for-multiple-testing" p-value (FDR) are provided for the individual probes.

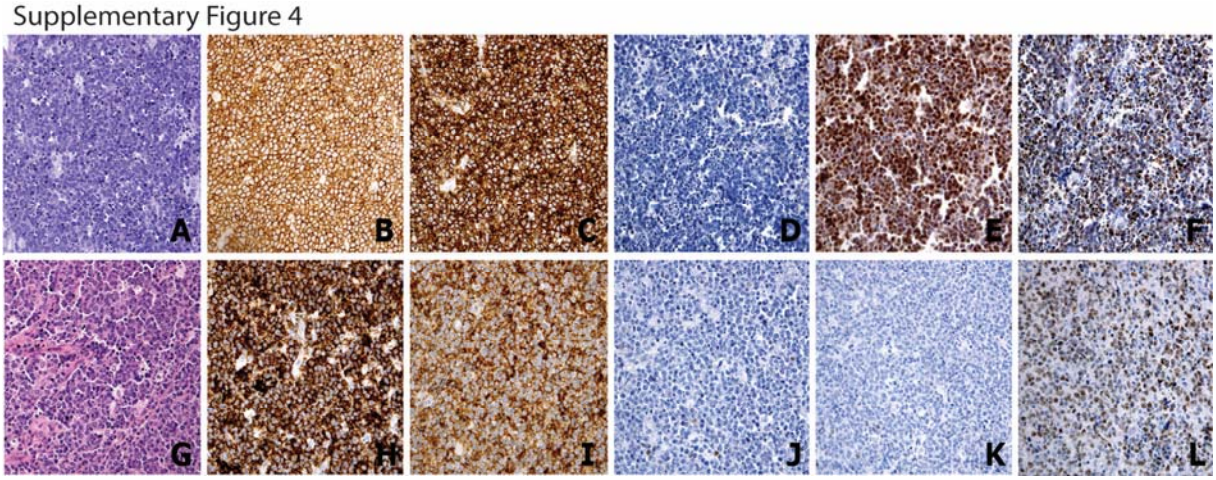

Supplementary Figure S4. Morphology and immunophenotype of ID-mBL. Images in the top and bottom rows represent *MYC*-translocation-positive case 4 and case 5 with the 11q-gain/loss pattern, respectively. (A) and (G), hematoxilin&eosin staining. In the remaining images, examples of immunohistochemistry for CD20 (B and H), CD10 (C and I), BCL2 (D and J), MYC (E and K) and Ki67 (F and L). The images were taken at 200x and then scaled.

Supplemental Table S1. Differentially expressed genes in MGR (red) and MLR (green).

probe set id	Gene Symbol	Gene Title	11q+/- vs t[MYC] FoldChange	11q+/- vs t[MYC] PValue	Chromosome	Start	End	Chromosomal band
224777_s_at	PAFAH1B2	platelet-activating factor acetylhydrolase 1b, catalytic subunit 2 (30kDa)	1,5121	7,88E-05	chr11	117015043	117041759	chr11q23
202038_at	UBE4A	ubiquitination factor E4A	2,1626	0,0335	chr11	118230358	118269922	chr11q23.3
208745_at	ATP5L	ATP synthase, H+ transporting, mitochondrial Fo complex, subunit G	1,8159	0,0432	chr11	118272103	118280562	chr11q23.3
208746_x_at	ATP5L	ATP synthase, H+ transporting, mitochondrial Fo complex, subunit G	1,5583	0,0282	chr11	118272320	118279908	chr11q23.3
210453_x_at	ATP5L	ATP synthase, H+ transporting, mitochondrial Fo complex, subunit G	1,5499	0,0342	chr11	118272321	118279914	chr11q23.3
207573_x_at	ATP5L	ATP synthase, H+ transporting, mitochondrial Fo complex, subunit G	1,5705	0,0358	chr11	118272330	118279910	chr11q23.3
218483_s_at	IFT46	intraflagellar transport 46 homolog (Chlamydomonas)	2,3249	0,0091	chr11	118415260	118436714	chr11q23.3
201176_s_at	ARCN1	archain 1	2,7523	0,0114	chr11	118443147	118473613	chr11q23.3
225549_at	DDX6	DEAD (Asp-Glu-Ala-Asp) box helicase 6	1,3804	0,0222	chr11	118500744	118620182	chr11q23.3
227208_at	CCDC84	coiled-coil domain containing 84	2,6342	0,0394	chr11	118883892	118889035	chr11q23.3
200091_s_at	RPS25	ribosomal protein S25	1,3548	0,0359	chr11	118886429	118889326	chr11q23.3
203292_s_at	VPS11	vacuolar protein sorting 11 homolog (S. cerevisiae)	2,2357	0,0177	chr11	118938492	118952675	chr11q23
213344_s_at	H2AFX	H2A histone family, member X	1,8155	0,0209	chr11	118964583	118965076	chr11q23.3
205436_s_at	H2AFX	H2A histone family, member X	2,0447	0,0427	chr11	118964586	118966177	chr11q23.3
204757_s_at	C2CD2L	C2CD2-like	1,71	0,0475	chr11	118978783	118989043	chr11q23.3
206495_s_at	HINFP	histone H4 transcription factor	3,211	0,0171	chr11	118997642	119005764	chr11q23.3
1553695_a_at	NLRX1	NLR family member X1	2,2767	0,021	chr11	119039439	119054725	chr11q23.3
219680_at	NLRX1	NLR family member X1	2,2785	0,0016	chr11	119045428	119054723	chr11q23.3
229010_at	CBL	Cbl proto-oncogene, E3 ubiquitin protein ligase	2,6837	0,0246	chr11	119171132	119172744	chr11q23.3
225231_at	CBL	Cbl proto-oncogene, E3 ubiquitin protein ligase	2,0956	0,0272	chr11	119175481	119178857	chr11q23.3
225234_at	CBL	Cbl proto-oncogene, E3 ubiquitin protein ligase	1,9879	0,0279	chr11	119175481	119178857	chr11q23.3
229337_at	USP2	ubiquitin specific peptidase 2	25,2497	0,0118	chr11	119225924	119226401	chr11q23.3
207211_at	USP2	ubiquitin specific peptidase 2	1,372	0,0399	chr11	119227511	119234629	chr11q23.3
207213_s_at	USP2	ubiquitin specific peptidase 2	30,6986	0,0144	chr11	119227511	119234629	chr11q23.3
204327_s_at	ZNF202	zinc finger protein 202	-2,0264	0,0086	chr11	123594634	123612325	chr11q23.3
204329_s_at	ZNF202	zinc finger protein 202	-1,7887	0,034	chr11	123594634	123612325	chr11q23.3
225819_at	TBRG1	transforming growth factor beta regulator 1	-1,6264	0,0219	chr11	124492773	124502634	chr11q24.2
230320_at	TBRG1	transforming growth factor beta regulator 1	-1,4489	0,0304	chr11	124504861	124505294	chr11q24.2
235654_at	TMEM218	transmembrane protein 218	-1,6734	0,0319	chr11	124965539	124966001	chr11q24.2
226073_at	TMEM218	transmembrane protein 218	-1,6272	0,024	chr11	124966576	124981604	chr11q24.2
208289_s_at	EI24	etoposide induced 2.4 mRNA	-1,6532	0,0395	chr11	125439411	125454575	chr11q24
216396_s_at	EI24	etoposide induced 2.4 mRNA	-1,7454	0,0167	chr11	125452532	125454124	chr11q24
202223_at	STT3A	STT3, subunit of the oligosaccharyltransferase complex, homolog A (S. cerevisiae)	-1,9276	0,0081	chr11	125462741	125490953	chr11q23.3
221277_s_at	PUS3	pseudouridylate synthase 3	-1,9179	0,004	chr11	125763379	125766209	chr11q24.2
225398_at	RPUSD4	RNA pseudouridylate synthase domain containing 4	-2,1666	0,0062	chr11	126071990	126081531	chr11q24.2
223386_at	FAM118B	family with sequence similarity 118, member B	-1,5259	0,0477	chr11	126081698	126132460	chr11q24.2
223128_at	FOXRED1	FAD-dependent oxidoreductase domain containing 1	-1,8328	0,0025	chr11	126139054	126148026	chr11q24.2
1552804_a_at	TIRAP	toll-interleukin 1 receptor (TIR) domain containing adaptor protein	-1,4053	0,0153	chr11	126153001	126163130	chr11q24.2
218774_at	DCPS	decapping enzyme, scavenger	-2,0301	0,0227	chr11	126173969	126215644	chr11q24.2
224833_at	ETS1	v-ets erythroblastosis virus E26 oncogene homolog 1 (avian)	-1,402	0,0027	chr11	128328659	128332010	chr11q23.3
1555355_a_at	ETS1	v-ets erythroblastosis virus E26 oncogene homolog 1 (avian)	-1,3274	0,0412	chr11	128331389	128392160	chr11q23.3
214447_at	ETS1	v-ets erythroblastosis virus E26 oncogene homolog 1 (avian)	-1,3826	0,0064	chr11	128332071	128392248	chr11q23.3
214875_x_at	APLP2	amyloid beta (A4) precursor-like protein 2	-1,6967	0,049	chr11	129979330	130014283	chr11q24
202005_at	ST14	suppression of tumorigenicity 14 (colon carcinoma)	-1,9629	0,0261	chr11	130029839	130080256	chr11q24-q25
216905_s_at	ST14	suppression of tumorigenicity 14 (colon carcinoma)	-2,0863	0,0067	chr11	130058086	130080256	chr11q24-q25
226148_at	ZBTB44	zinc finger and BTB domain containing 44	-1,8138	0,0349	chr11	130100253	130131329	chr11q24.3
220243_at	ZBTB44	zinc finger and BTB domain containing 44	-2,3587	0,0376	chr11	130108974	130184321	chr11q24.3
202358_s_at	SNX19	sorting nexin 19	-1,3925	0,0414	chr11	130745773	130786362	chr11q25
202359_s_at	SNX19	sorting nexin 19	-1,5302	0,048	chr11	130745774	130786362	chr11q25
1554986_a_at	SNX19	sorting nexin 19	-1,4202	0,0304	chr11	130775552	130786344	chr11q25
212789_at	NCAPD3	non-SMC condensin II complex, subunit D3	-1,6052	0,0363	chr11	134022339	134093868	chr11q25
221669_s_at	ACAD8	acyl-CoA dehydrogenase family, member 8	-1,3771	0,0254	chr11	134123464	134135555	chr11q25